Journal of Power Sources 185 (2008) 698–710

Contents lists available at ScienceDirect

Journal of Power Sources

journal homepage: www.elsevier.com/locate/jpowsour

Aging of $LiFePO_4$ upon exposure to H_2O

K. Zaghib[a,*], M. Dontigny[a], P. Charest[a], J.F. Labrecque[a], A. Guerfi[a], M. Kopec[b], A. Mauger[c], F. Gendron[b], C.M. Julien[b]

[a] Institut de Recherche d'Hydro-Queĭbec, 1800 Boul. Lionel Boulet, Varennes, QC, Canada J3X 1S1
[b] UPMC Université Paris6, UMR 7588, Institut des Nano-Sciences de Paris, 140 rue de Lourmel, 75015 Paris, France
[c] UPMC Université Paris6, UMR 7590, Institut de Mineĭralogie et Physique de la Matieère Condenseĭe, 140 rue de Lourmel, 75015 Paris, France

ARTICLE INFO

Article history:
Received 5 July 2008
Received in revised form 29 July 2008
Accepted 19 August 2008
Available online 22 August 2008

Keywords:
Lithium-ion
Cathode
$LiFePO_4$
Aging
H_2O

ABSTRACT

The effect of H_2O on carbon-coated $LiFePO_4$ particles was investigated by chemical analysis, structural analysis (X-ray diffraction, SEM, TEM), optical spectroscopy (FTIR, Raman) and magnetic measurements. Upon immersion in water, part of the product floats while the main part sinks. Both the floating and the sinking part have been analyzed. We find that the floating and sinking part only differ by the amount of carbon that partly detaches from the particles upon immersion in water. Exposure to H_2O results in rapid attack, within minutes, of the surface layer of the particles, because the particles are no longer protected by carbon. The deterioration of the carbon coat is dependent on the synthesis process, either hydrothermal or solid-state reaction. In both cases, however, the carbon coat is permeable to water and fails to protect the surface of the $LiFePO_4$ particles. The consequence is that this immersion results in the chemical attack of $LiFePO_4$, but is restricted to the surface layer of the particles (few nanometers-thick). In case the particles are simply exposed to humid air, the carbon coat protects the particles more efficiently. In this case, the exposure to H_2O mainly results in the delithiation of the surface layer, due to the hydrophilic nature of Li, and only the surface layer is affected, at least for a reasonable time of exposure to humid air (weeks). In addition, within this timescale, the surface layer can be chemically lithiated again, and the samples can be dried to remove the moisture, restoring the reversible electrochemical properties.

1. Introduction

The utility of lithium iron phosphate $LiFePO_4$ as a positive electrode material in lithium-ion batteries was reported 10 years ago [1]. The main controversy with this material is its the low electronic conductivity, for reasons that were discussed elsewhere [2]. It was observed that coating of the $LiFePO_4$ particles with conductive carbon [3–5] solved this problem, and now $LiFePO_4$-based Li-ion batteries are found in commercial products where they have definitive advantages in some applications [1,4,5]. In addition, it is non-toxic compared to compounds including cobalt. Currently, $LiFePO_4$ is prepared without impurities that have hindered its electrochemical performance in the past [6,7]. Thus $LiFePO_4$ is produced on a large scale with a capacity close to theoretical, 170 Ah kg^{-1} [1].

The extensive use of $LiFePO_4$ worldwide, however, requires further investigation of abuse tolerance, which requires expensive protections for Li-ion batteries. $LiFePO_4$ already has a remarkable thermal stability, but its aging properties need to be explored further. The impact of ambient air exposure has been investigated recently. In particular, degradation of the voltammetric performance of $LiFePO_4$ in air was detected after a few weeks and up to 1 year [8]. The presence of impurities that may be produced, not only during sintering, but also during storage in ambient air [7,9], is responsible for aging and a decrease in the specific capacity [10]. More recently, changes to the surface of the $LiFePO_4$ particles on the time scale of 1 day in air [11,12] was observed. On this shorter time scale, the changes are expected to only cause partial de-intercalation of lithium rather than the formation of an impurity phase, so that only the first cycle of the battery is affected [11]. It is not clear, however, whether these effects are due to the humidity of the ambient atmosphere, or oxygen, inasmuch as lithium reacts with many components of the atmosphere. The best evidence for the reactivity of Li metal exposed to ambient atmosphere is the formation of a mixture of lithium hydroxide (LiOH), lithium carbonate (Li_2CO_3), and lithium nitride (Li_3N) [13]. We show in this work that the reactivity of lithium with formation of LiOH and Li_2CO_3 is still observed for Li in $LiFePO_4$ in contact with water, although the

* Corresponding author. Tel.: +1 450 652 8019; fax: +1 450 652 8424.
E-mail address: zaghib.karim@ireq.ca (K. Zaghib).

0378-7753/$ – see front matter © 2008 Elsevier B.V. All rights reserved.
doi:10.1016/j.jpowsour.2008.08.028

kinetics and thermodynamics are certainly different from the case of Li metal.

It is well known that all lithium-ion batteries need to be protected against humidity. The main reason is that lithium is very reactive with water, according to the chemical reaction:

$$Li + H_2O \rightarrow LiOH + 1/2H_2 \quad (1)$$

Lithium hydroxide (LiOH) is a corrosive alkali hydroxide that crystallizes to a white hygroscopic material. It is soluble in water, a property that has been used to investigate aqueous LiOH as a potential electrolyte in Li-ion batteries with a $LiFePO_4$ cathode [14]. Since the carbon coat is not a barrier for Li^+ ion transport (the reason for the success of C-$LiFePO_4$ as a cathode element of Li-ion batteries), we expect reaction (1) to be effective, implying extraction of Li from $LiFePO_4$ to interact with water. As we shall see in the present work, delithiation is observed in the case of exposure to H_2O in air, and yet, it affects only the disordered surface layer of the $LiFePO_4$ particles.

Despite the reaction of lithium to humidity, we immersed the $LiFePO_4$ particles in water to check the effectiveness of the carbon-coating process by separating coated and uncoated particles [15]. This means of characterization is based on the fact that, when the C-$LiFePO_4$ powder is exposed to liquid water, part of the carbon that links the particles detaches and floats to the surface, retaining with it some $LiFePO_4$, while the major part sinks. More recently, Porcher et al. determined that exposure of C-$LiFePO_4$ particles to water results in the formation of a thin layer of Li_3PO_4 (few nm thick) at the surface of the particles [16], as a result of the migration of Fe into the water. In the present work, we investigated the effect of water on carbon-coated $LiFePO_4$ particles and analyzed both the particles that have sunk and the particles that float on water.

A strong interaction between $LiFePO_4$ with H_2O molecules was not necessarily expected. After all, corrosion protection of iron is an industrial process that amounts to dropping iron into a hot bath including manganese phosphide, which results in the formation of a thin layer of $FePO_4$ at the surface. Since iron phosphate is hydrophobic, this layer protects the iron against oxidation and corrosion. Intuition would suggest that, upon immersion of $LiFePO_4$ into water, delithiation in a thin layer at the surface would lead to the formation of a $FePO_4$ layer that would protect the particles against any other damage. [17,18]. The carbon coating might also play an important role in determining the stability of the underlying $LiFePO_4$ sample in humid conditions. We actually have detected that the carbon coating changes very much the surface layer, as reported in Ref. [19]. Our present investigations, however, show that the situation is slightly more complicated.

The contents of this paper are arranged as follows. In the next section, experimental details are reported, together with the sample preparation. The next section is devoted to the characterization of the sample before and after immersion in water. Both the floating parts and the sinking parts were characterized by XRD, scanning electron microscopy (SEM) and transmission electron microscopy (TEM). Their composition was analyzed by FTIR and magnetic measurements in relation to the electrochemical properties, as a function of the time exposed to water. We also report the chemical analysis of the aqueous solution provide us with some insight into the reaction of $LiFePO_4$ with water. Since immersion in water is a rather dramatic event that does not give any opening to the carbon coat to isolate the $LiFePO_4$ surface from H_2O molecules, we have also explored the case where the material is only exposed to humid ambient air. Finally, we also report on the hydroscopic nature of $LiFePO_4$ and the consequence on the degradation of the electrochemical performance of this material upon exposure to ambient atmosphere for a few months.

2. Experimental

2.1. Sample preparation

The C-$LiFePO_4$ samples used were prepared by two different chemical routes: solid-state reaction (hereafter called sample SSR), and hydrothermal (HTR). The SSR-$LiFePO_4$ was prepared from $FePO_4(H_2O)_2$ and Li_2CO_3. The stoichiometric amounts of precursors were thoroughly mixed in isopropanol. After drying, the blend was heated at 700 °C under a reducing atmosphere, i.e., argon +5% hydrogen, for 6 h. C-$LiFePO_4$ was prepared from the $LiFePO_4$-SSR sample, with sucrose and cellulose acetate as the carbon precursors in acetone solution according to the procedure described by Ait Salah et al. [21].

In the second method, $LiFePO_4$ (HTR) was synthesized using the hydrothermal process pioneered by Zaghib and Armand [22] and in subsequent publications [23]. Equimolar amounts of $FeSO_4$ and H_3PO_4 were mixed in deoxygenated and deionized water. A small amount of citric acid was added to the mixture to prevent iron oxidation. A 0.19-M LiOH solution was added slowly to give Fe:P:Li equal to 1:1:3. After stirring under nitrogen for about 5 min, the reaction mixture was transferred to a Parr reactor, which was purged with nitrogen and held at 180–220 °C for 3–5 h. On cooling to room temperature, the precipitate was filtered and thoroughly washed with deionized water and dried at 85 °C for 24 h in a special glove box using vacuum-nitrogen scan. The particles that floated in water were referred to as "floating particles". The other particles that were removed from the bottom of the water container are referred to as "sinking particles". The carbon contents of the hydrothermal and solid state LFP products were measured at 1.1 wt.%.

2.2. Apparatus

The crystal structure of LFP samples was analyzed by X-ray diffractometry (XRD) using a Philips X'Pert apparatus equipped with a Cu Kα X-ray source (λ = 1.5406 Å). XRD measurements were collected in the 2θ range 10–80°. FTIR absorption spectra were recorded with a Fourier transform interferometer (model Bruker IFS113v) in the wavenumber range 150–1400 cm^{-1} at a spectral resolution of 2 cm^{-1}. The samples were ground to fine powders and dispersed into a CsI pellet in the proportion (1:300).

Scanning electron microscopy (SEM) coupled with an energy dispersive X-ray analyzer (EDX) was used to study the morphology. The SEM images were collected using a Hitachi S-4700 microscope in the ultra-high-resolution mode. Transmission electron microscopy (TEM) images were obtained with an electron microscope (Hitachi model H-9000) working at a potential of 300 kV. The TEM samples were ultrasonically treated in a solution of isopropylic alcohol and then deposited on silica substrate.

The granulometry of the powder was measured with the Partica LA-950V2 Laser Diffraction Particle Size Analyser (HORIBA Instruments).

FTIR absorption spectra were recorded with a Fourier transform interferometer (model Bruker IFS113 vacuum interferometer) in the wavenumber range 150–1400 cm^{-1} with spectral resolution 2 cm^{-1}. In the far-infrared region (400–100 cm^{-1}), the vacuum bench apparatus was equipped with a 3.5-μm thick Mylar beam splitter, a globar source and a DTGS/PE far-infrared detector. For such measurements, the powders were grounded with CsI and pressed into translucent disks.

Magnetic measurements (susceptibility and magnetization) were carried out with a fully automated magnetometer (MPMS-5S from Quantum Design) using a ultra-sensitive Superconducting Quantum Interference Device (SQUID) in the temperature range

4–300 K. Powders were placed into small plastic vial, placed in a holder and finally inserted into the helium cryostat of the SQUID apparatus.

The moisture of the material in air was measured with a Computrac moisture analyzer (Arizona Instruments LLC).

The electrochemical properties were measured in cells with metallic lithium as the negative electrode. The electrode was 1 M $LiPF_6$ in ethylene carbonate (EC) + diethylene carbonate (DEC). The electrochemical studies were conducted at different temperatures (25, 45 and 60 °C).

3. Results

3.1. Structural properties

Before immersion in water, the XRD data (not reported) only shows spectral lines characteristic of $LiFePO_4$ in the olivine structure. The SEM images of the samples are shown in Fig. 1. The powder of the HTR sample consists of ellipsoidal-shaped particles with a typical size of the order of 0.4 μm. The non-spherical shape of submicron particles was previously observed and explained as a result of the geometry of the olivine structure [18,19]. Bigger particles, however, can also be seen in the picture, suggesting aggregation of the former particles stuck together. Sub-micron particles can also be seen in SEM images of the SSR sample. The main difference between the two samples is the larger amount of aggregates in the HTR sample, so the average size of these particles is larger.

This image of the $LiFePO_4$ particles was confirmed by the granulometry of the samples, shown in Fig. 2. The size distribution of HTR particles shows a first peak centered at 0.39 μm, followed by a tail that goes through a secondary maximum at 10 μm. On the other hand, the size distribution of the SSR sample is very broad, extending continuously from 0.25 to 20 μm. The shape of the larger particles is complex, and is the best evidence that they are formed from smaller particles of ellipsoidal shape that are stuck together, rather than individual large particles that have a more spherical shape.

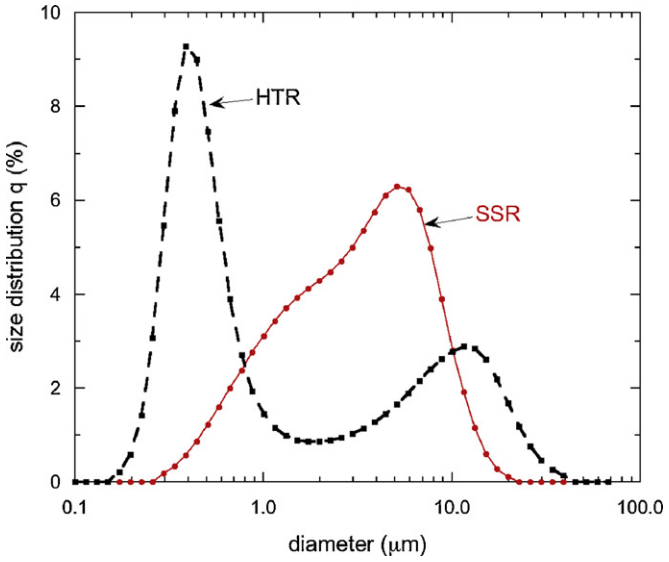

Fig. 2. Granulometry of the SSR and HTR $LiFePO_4$ samples.

The high-resolution TEM image of one particle before immersion (see Fig. 3) shows the carbon coat, a few nm-thick, on top of the surface of $LiFePO_4$. The TEM shows the presence of a disordered layer nearly 3.5-nm thick, in agreement with other results [20].

After immersion of $LiFePO_4$ particles in water, most of the particles sink, as expected for particles that have a density higher than one. However, part of the sample floats. This is illustrated in Fig. 4.

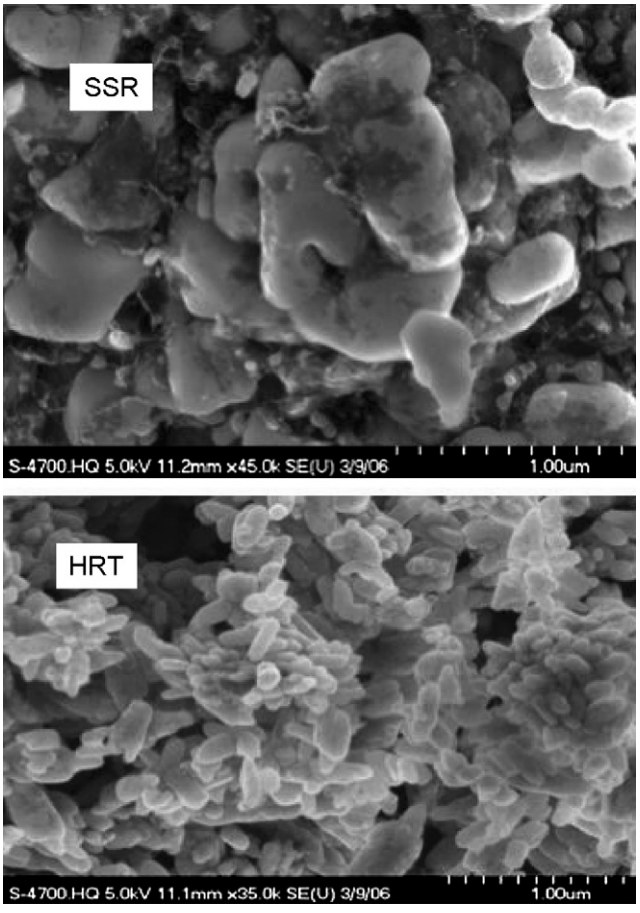

Fig. 1. SEM images of SSR and HTR $LiFePO_4$ samples before immersion in water.

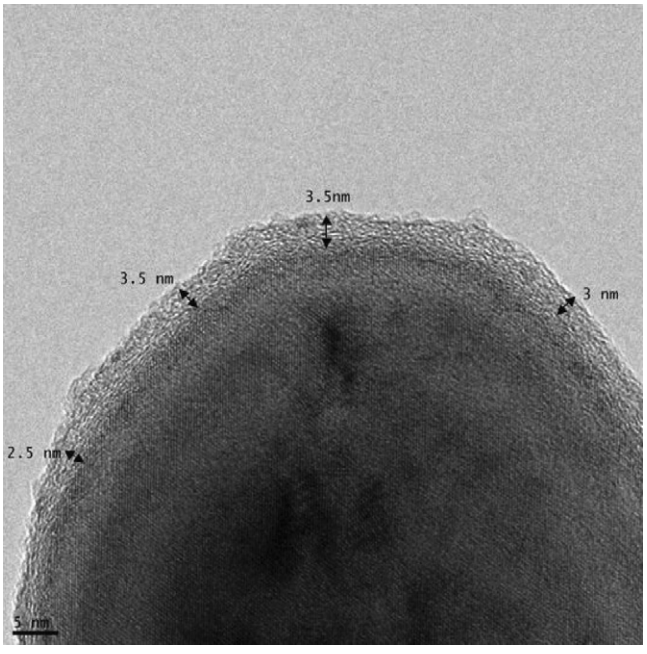

Fig. 3. TEM image of a carbon-coated $LiFePO_4$ particle before immersion (particle of SSR sample, but the same is observed for HTR sample).

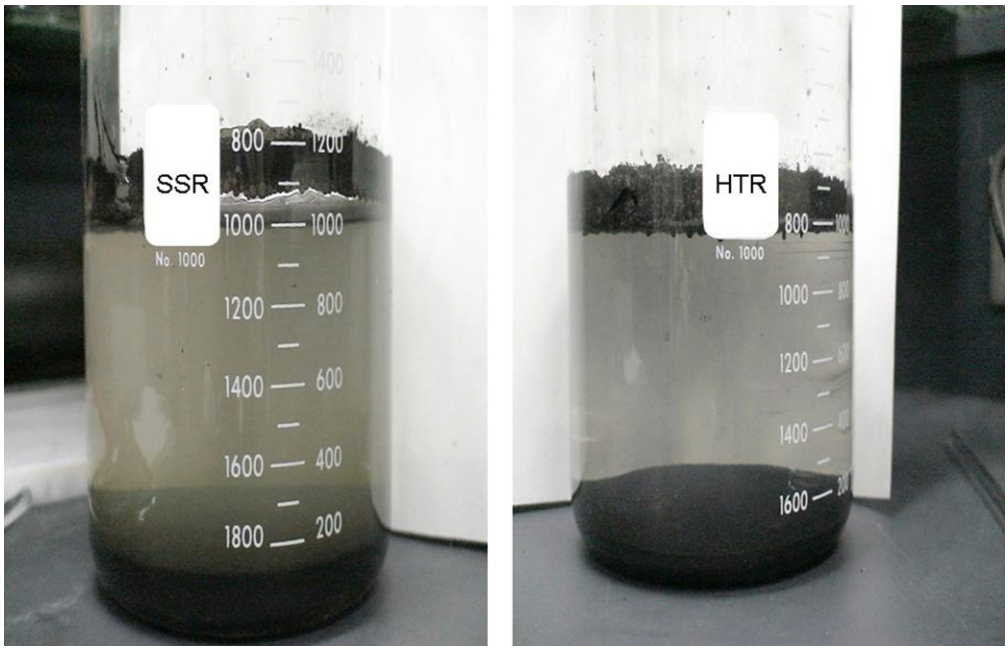

Fig. 4. SSR and HTR $LiFePO_4$ samples after immersion during 2 days in water.

Since the Brownian motion for such big particles is negligible, the floating part cannot be attributed solely to $LiFePO_4$ particles. We investigated its composition by EDX suitable to chemical analysis of insulating materials. The results are illustrated in Fig. 5 for the sample SSR, together with the EDX spectrum of the sinking part, for comparison. Similar results (not reported) were obtained for the HTR sample. The chemical elements are readily identified by the EDX peaks corresponding to the binding energy of the C(1s), O(1s) Fe(2p) electrons [24]. The ratios of the Fe, O and P elements as determined from the peak intensities are in agreement with the chemical composition of iron phosphate with the formula $LiFePO_4$. The only difference is the larger amount of carbon in the floating part, as evident from the much larger intensity of the carbon peak in the EDX spectrum. The HRTEM image of the floating part reported in Fig. 6 shows that it is essentially carbon fibers to which are attached $LiFePO_4$ particles that have lost part of their carbon coat upon immersion in water. This observation provides an explanation of why these particles float. Before immersion in water, the carbon holds the particles together (the very reason why it insures the electronic conductivity between the particles), and coats the particles. Upon immersion in water, the adherence of the carbon coat to the particles decreases, at least on part of the surface. As a result, part of the carbon detaches and floats to the surface of the water due to its surface tension. Some particles, remain stuck to the floating carbon, but are too small to sink. However, the TEM images show unambiguously that the $LiFePO_4$ particles, even in this carbon-rich medium, have lost their carbon coating, and are tied to the carbon only locally on their surface.

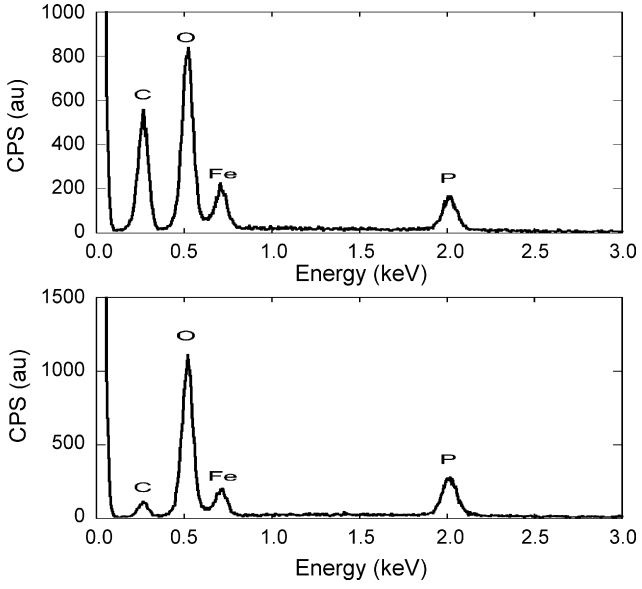

Fig. 5. EDX spectra of the floating (upper curve) and sinking part (lower curve) of the SSR $LiFePO_4$ sample after immersion during 2 days in water.

Fig. 7 shows the SEM images of the SSR and HTR samples that sink in water. Both of these images indicate a less dispersed size-distribution of the particles. For the majority of particles smaller than 1 μm in the SSR sample, it appears that the bigger particles prior to immersion are actually aggregates of smaller ones that separated from each other during the immersion process. However, few aggregates subsist. This is expected, and a general property that is not specific to $LiFePO_4$. Brownian motion of nm-sized particles, and surface treatments that favor their stability in colloidal suspension, is not sufficient to prevent the formation of aggregates that reduces the formation of mono-disperse particles [25].

The XRD spectra of SSR-$LiFePO_4$ particles, illustrated in Fig. 8, indicate samples from the floating and sinking part after 1 h in water do not differ significantly from the XRD spectrum before immersion in water. The lattice parameters are not significantly modified either, as illustrated in Fig. 9, where the crystallographic parameters a and b are reported after different times of exposure to water. For all samples, irrespective of the time spent in water, $a = 10.333(5)$ Å, $b = 6.006(4)$ Å, $c = 4.703(5)$ Å, while the unit cell volume is $291.8(7)$ Å^3. These parameters are evidence that the bulk of the $LiFePO_4$ particles is unaffected by water, only the surface layer is affected. However, XRD is not sufficiently sensitive to probe this surface layer for two reasons: the surface/volume ratio is too small

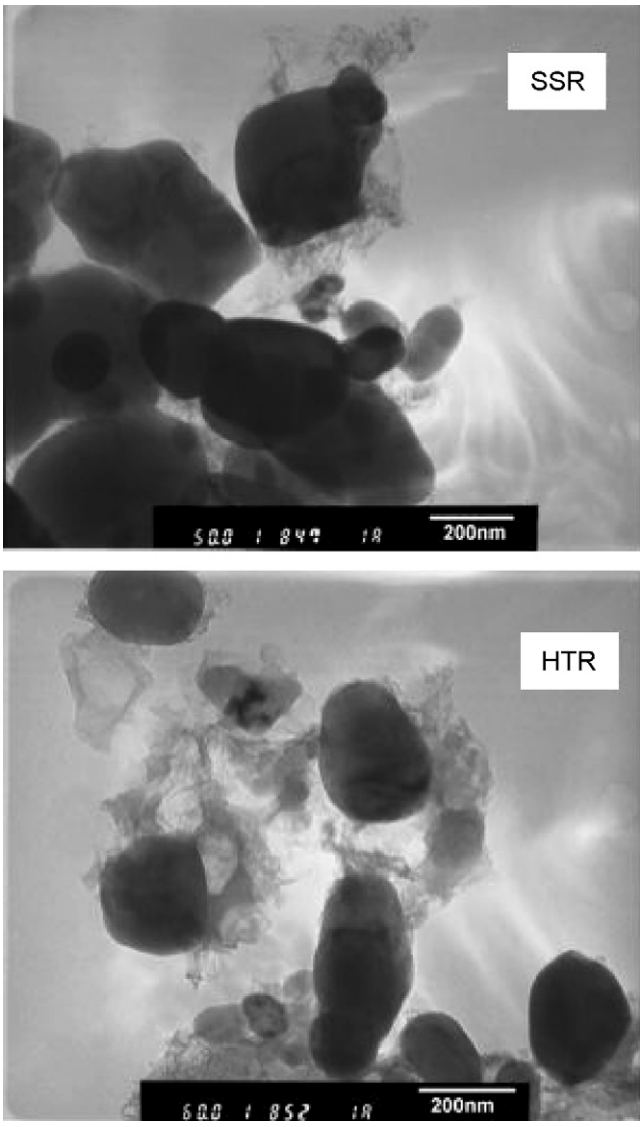

Fig. 6. TEM image of the floating part of SSR $LiFePO_4$ sample.

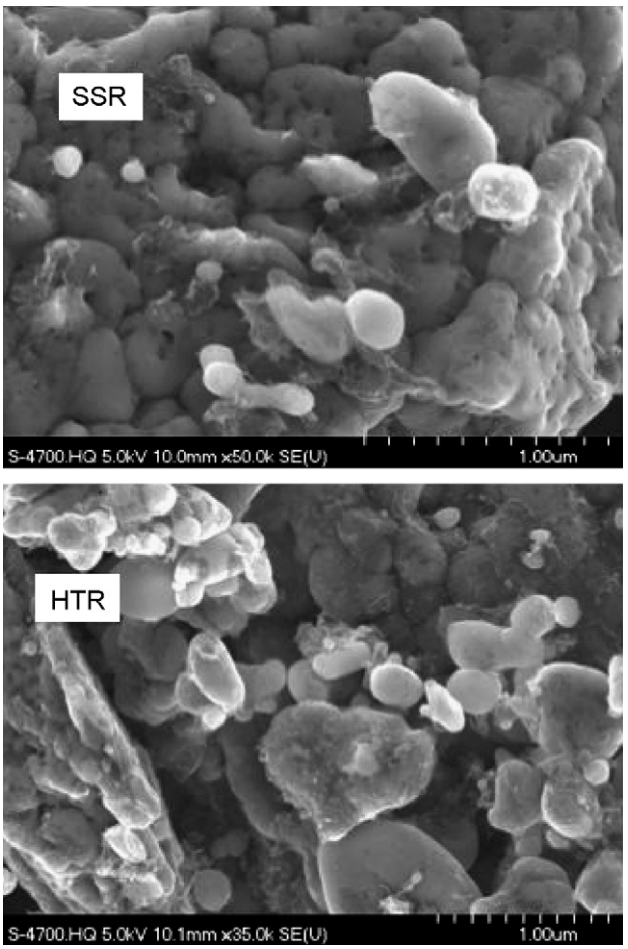

Fig. 7. SEM images of the sinking part of SSR and HTR $LiFePO_4$ samples.

for these big particles, and the surface layer is disordered. Therefore, detecting changes in the surface by water will require other types of experiments.

3.2. Water analysis

$LiFePO_4$ reacts with H_2O, particularly with the SSR sample, which is evident by the yellow color in the water (see Fig. 4). The HTR sample appears to be less reactive, since the water remains uncolored. Note, however, that this attack is not related to impurity phases, because we know how to detect impurity phases when they exist, from magnetic plus FTIR experiments (see our prior work [2] and refs herein). From these analyses that we performed before exposure to moisture, we know that there is no impurity phase in these samples (except for a residual concentration of Fe_2O_3 for one sample only, as will be shown below).

A more quantitative characterization of the reaction of the samples with water is provided by inductively coupled mass (ICM) spectroscopy analysis of the liquid in which the SSR- and HTR-$LiFePO_4$ samples are immersed. For comparison, the same experiments were performed with the samples immersed in *N*-

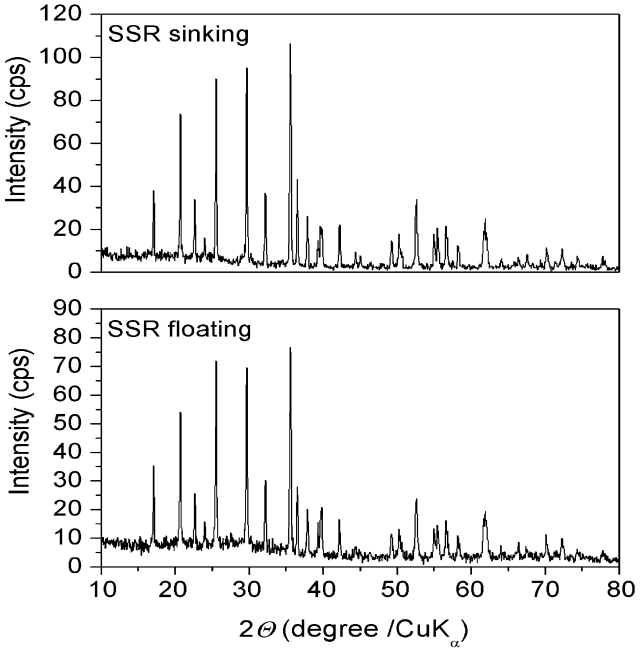

Fig. 8. XRD spectra of the floating part and sinking part of SSR $LiFePO_4$ sample, after spending 1 h in water.

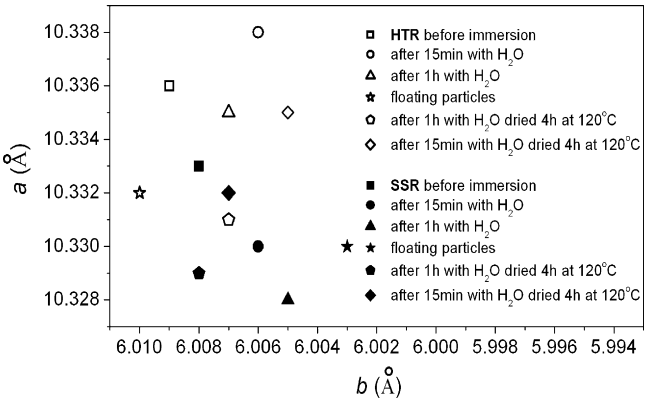

Fig. 9. Lattice parameters *a* and *b* for both SSR and HTR $LiFePO_4$ particles. The data labeled "SSR" and HTR" are obtained before immersion in water. The other results have been obtained after different treatments indicated in the figure. When the label "floating" is indicated, it means that the result has been obtained for the floating part of the sample, otherwise the result is for the sinking part.

methylpyrrolidone (NMP), since this solvent is generally used to dissolve poly(vinylidene fluoride) (PVdF) which is widely adopted as a binder for electrodes manufactured for Li-ion cells. The results are summarized in Table 1. The same amount of sample and volume of liquid (either NMP solvent or water) were used in all experiments, so the results can be compared quantitatively. The amount of P and Fe ions in the liquid is negligible (a few ppm only) in the case of immersion in NMP, from which we conclude that $LiFePO_4$ does not react. On the other hand, the amount of P and Fe detected in the liquid increased by almost two orders of magnitude when NMP is replaced by water.

The water analysis (composition) is quantitative, and it is already an improvement, since it has not been done before. However, the data are still not sufficient to identify the nature of the chemical products that have been formed. Nevertheless same hypotheses can be made based upon general considerations. The water in which the HTR sample was immersed remains transparent despite the presence of soluble Fe and P species. If the phosphate [PO_4^{3-}] ion is conserved in the dissolution process, the formation of lithiophosphate Li_3PO_4 cannot be the dominant process because it is not soluble in water. There are different iron phosphate complex ions, either ferric or ferrous. As mentioned above, ferric phosphate [$FePO_4$] is 'waterproof', and should stay at the surface of the particles to protect them against further dissolution. This will be confirmed by an analysis of its physical properties. Ferrous phosphate [$Fe_3(PO_4)_2$], which is found in numerous minerals [$Fe_3(PO_4)_2{\cdot}nH_2O$, ludlamite ($n = 2.4$), vivianite (up to $n = 8$)], is also unexpected because the ratio of P:Fe in water is $[P]/[Fe] = 2.5 \pm 0.2$ (see Table 1), and ferrous phosphate has a ratio less than one. The large value of [P]/[Fe] does not preclude the formation of such materials, but it actually requires that P is dominantly in lower-charged complex ions that form in aqueous solution: hydrogen phosphate ion [HPO_4^{2-}], dihydrogen phosphate ion [$H_2PO_4^-$]. Aqueous phosphoric acid [H_3PO_4] is ruled out by the fact that the pH of the aqueous solution in which the SSR and HTR samples were immersed is basic, namely 9.5 in both cases. Indeed, $Fe(H_2PO_4)_2$ is soluble in water. In addition, this material is formed during the phosphatation of iron, an industrial process used to passivate the surface of iron compounds [26]. Lithium reacts with the water to form LiOH that is soluble. In addition, Li can also react with carbon to form $LiCO_3$ that is also soluble. Note that the formation of $Fe(H_2PO_4)_2$ leads to $[P]/[Fe] = 2$. This value is only slightly smaller than the experimental value, but still the difference exceeds the experimental uncertainty. There should then be a residual concentration of another phosphate species that does not involve the iron element. This may be the footprint a small amount of Li_3PO_4 particles in suspension in the aqueous solution. For instance, in the aqueous solution with HTR, where $[P]/[Fe] = 2.3$, we can envision a corrosion reaction that would satisfy this ratio:

$$LiFePO_4 + H_2O \rightarrow Fe(H_2PO_4)_{2(aq)} + 1/3[Li_3PO_4] \quad (2)$$

This reaction is certainly not sufficient to summarize the whole corrosion process, as exemplified by the reaction in Eq. (2) associated to the formation of LiOH. The amount of lithium phosphate particles, if any, must be low enough that it does not affect the transparency of the solution (see right side of Fig. 4).

Table 1
Inductively coupled mass spectroscopy analysis of the liquid in which the SSR and HTR $LiFePO_4$ samples have been immersed

Sample	NMP after 24 h		H_2O after 24 h	
	Fe (ppm)	P (ppm)	Fe (ppm)	P (ppm)
SSR	6.2	6.3	150	400
HTR	0.3	2.3	130	300

The same amount of product, and same volume of liquid (either NMP solvent or water) has been used in both cases, so the results can be compared quantitatively. These results have been obtained in a standard procedure according to which 50 g of initial C-$LiFePO_4$ product is immersed in 600 ml of liquid (water or NMP).

3.3. Analysis of the deposit after evaporation

Fig. 10 shows the deposit after evaporation of the water in which the samples were immersed. In this experiment, the floating part was removed, before evaporating the solution, so the deposit consists of the sample that has sunk, plus the part of material that was dissolved in water. The color of this deposit is almost black with blue iridescence in some areas of the SSR sample, but white for the HTR sample. The significant differences between the two samples are the distribution size (see Fig. 2), and the carbon deposit (see the sample preparation). In both samples, the particles are larger than 100 nm, and no quantum effect on the electronic structure is expected for such large particles. The particles are considered big enough that size is not the pertinent parameter. The difference observed in Fig. 10 must then come from carbon. Since part of the carbon floats while another part sinks when the samples are immersed in water, part of the carbon can be in the intermediate position, i.e., in suspension in the water. The presence of suspended carbon particles in solution is evident from the turbidity of the colored solution in which the SSR sample has been immersed (see Fig. 4). Upon drying, this carbon in suspension will deposit at the bottom of the container, forming a black crust. This is in essence the origin of the black color of the deposit in the case of the SSR sample. The blue iridescence is also observed at the surface of iron after phosphatation mentioned earlier, in which case it is attributed to the diffraction of light in the ultra-thin layer. The same effect is presumably the cause for the iridescence observed here. On the other hand, carbon does not form particles in suspension with the HTR sample, as evident by the transparency of the solution of the right side of in Fig. 4. The consequence is that the product decanted by evaporation of the solution in this case is mainly LiOH, in addition to the iron compounds mentioned above. The presence of LiOH and Li_2CO_3 were also detected by Raman spectroscopy as reported below. Both LiOH and Li_2CO_3 are white minerals, and give this color to the residue of the HTR deposit.

Further support for this analysis is provided by Raman spectroscopy which detects the presence of carbon due to the two characteristic Raman bands in the 1200–1700 cm^{-1} spectral range.

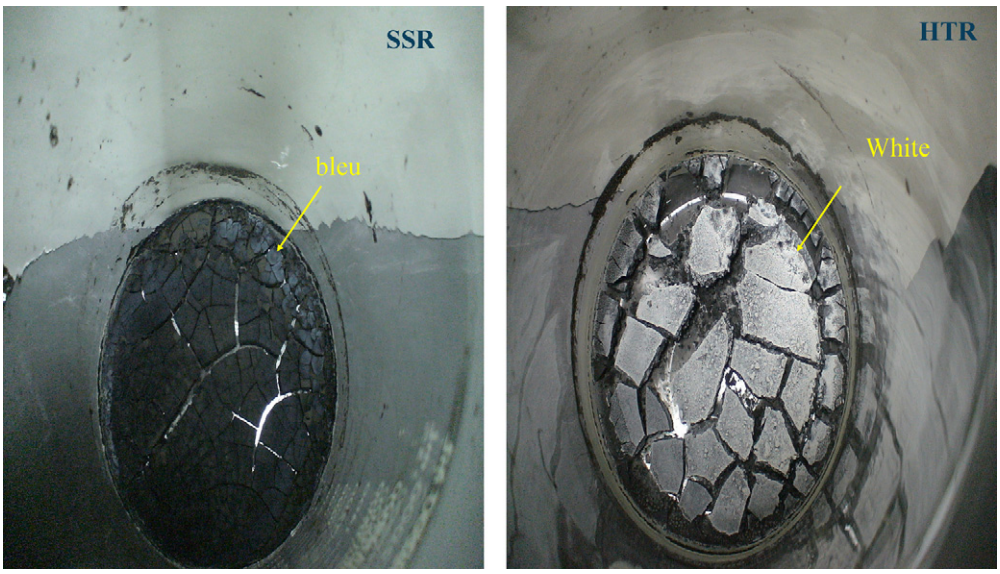

Fig. 10. Deposit obtained after removing the floating part, and evaporation of the water in which the $LiFePO_4$ samples SSR (left) and HTR (right) have been immersed.

The Raman spectra of the black/blue deposit (SSR) and white deposit (HTR) were measured with He–Ne laser (wavelength 632.8 nm). The result is illustrated in Fig. 11 for the black/blue SSR deposit. The spectrum of uncoated $LiFePO_4$ particles is also presented for comparison. While the intrinsic spectrum of $LiFePO_4$ is dominated by the peak at 960 cm^{-1} associated with the stretching mode of the PO_4 unit, the Raman spectrum of the part that shows blue iridescence is dominated by the two bands characteristic of carbon. The peak centered at 960 cm^{-1}, however, is distinctly visible, so this part of the specimen also contains phosphate. The Raman spectrum of the black part that does not show blue iridescence exhibited the dominant bands characteristic of carbon, but not the spectrum at 960 cm^{-1}. This series of spectra confirmed that the blue iridescence is associated with the presence of phosphate and a phosphatation effect. In addition, three bands are evident at lower frequencies, 398, 263 and 219 cm^{-1}, that are characteristic of $LiOH{\cdot}H_2O$ [28]. A broad band is observed in the vicinity of 1070 cm^{-1}, which is also detected in the part with blue iridescence. This broad line has been also detected in the Raman spectrum of molten LiOH and is attributed to the vibration of the CO_3 molecular unit [28], which confirms the presence of Li_2CO_3, in addition to LiOH. This is actually expected since Li_2CO_3 is by-product of LiOH reacting with the CO_2 of the atmosphere according to the equation ($2LiOH + CO_2 \rightarrow Li_2CO_3 + H_2O$).

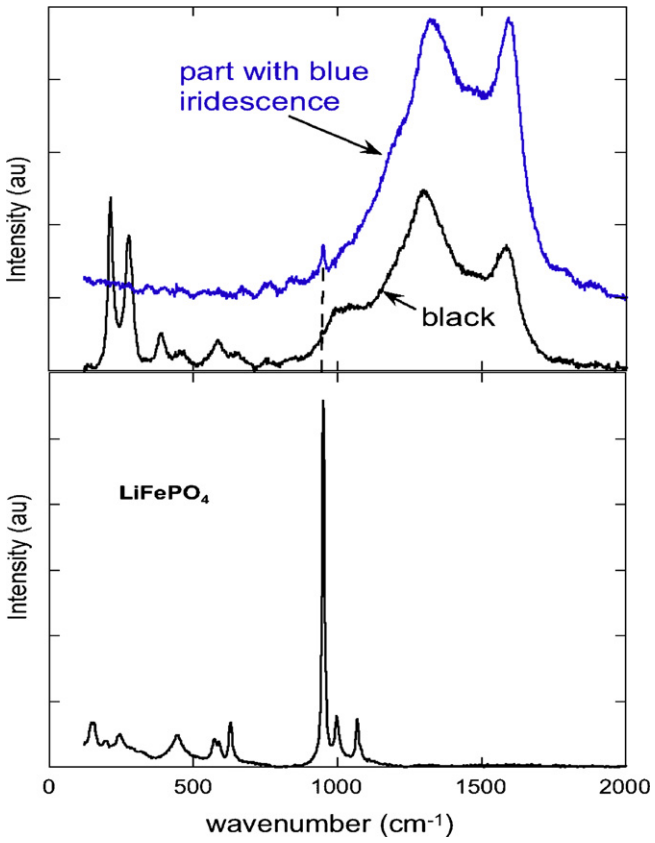

Fig. 11. Raman spectrum of the deposit shown in Fig. 10, for SSR $LiFePO_4$ sample. Black refers to the black part, and blue to the part that shows blue iridescence. The spectrum of uncoated $LiFePO_4$ is shown for comparison. The vertical broken line points to the position of the stretching mode of PO_4 units.

Of course, the carbon bands are absent from the Raman spectrum of the white part of the white deposit for the HTR sample, and the spectrum (not shown here) is flat in the 1200–1700 cm^{-1} spectral range.

3.4. Physical properties of the $LiFePO_4$ particles

FTIR is a useful tool to probe the local composition of the surface layer because the vibrations of the molecular units of the $LiFePO_4$ lattice are responsible for absorption bands in the spectrum even when the material is disordered [29]. In the present case, however, we could not detect significant variations upon immersion in water. For sinking particles, the spectrum remains unchanged after the sample was immersed in water for 1 h. This result is illustrated in Fig. 12 for the SSR sample. This spectrum is characteristic of $LiFePO_4$ and is described in detail elsewhere [30]. All the bands can be identified as intrinsic vibrations in $LiFePO_4$ [31,32]. For the case of the floating particles, the spectrum in the figure shows very little difference. The larger amount of carbon associated with the floating particles generate an additional diffusion. As a consequence, the spectrum is slightly noisier, which affects the band intensities of

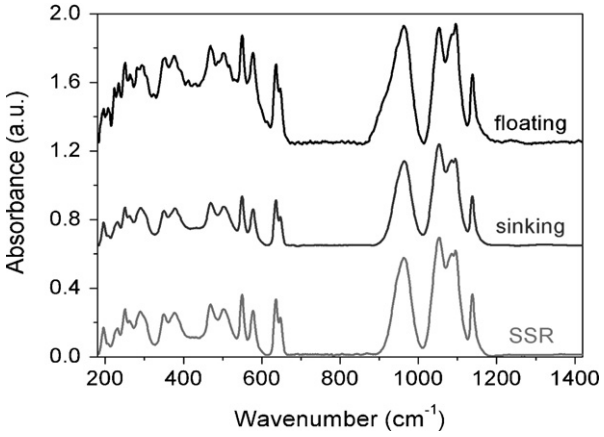

Fig. 12. FTIR spectra of the SSR $LiFePO_4$ sample before immersion in water (lowest curve), and for the sinking and floating parts after 1 h immersion in water.

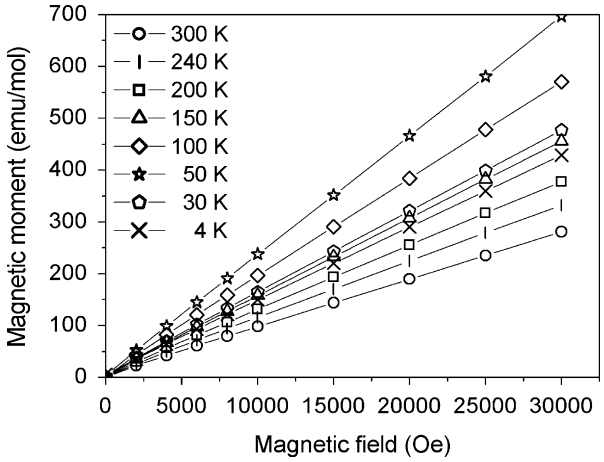

Fig. 13. Magnetization curves of the HTR $LiFePO_4$ sample before immersion.

the PO_4 vibrations. The only additional structure is a band of small intensity extending from 1220 to 1250 cm^{-1}. This band is characteristics of C—O—C stretch and asymmetric C—O stretch [33], and can then be attributed to the excess of carbon linked to oxygen in the floating part of the product (Fig. 4). The lack of sensitivity of the FTIR spectra in these experiments is further evidence that the reaction of the particles with water remains a surface effect. We observe the presence of Li_3PO_4 at the surface of the particles, identified by the characteristic band around 460 cm^{-1} [28]. However, even if such a layer exists, its detection by FTIR is unlikely for two reasons. First, the vibrations of the PO_4 units dominate the spectrum of Li_3PO_4 [27], and they are in common with $LiFePO_4$. Second, the surface/volume ratio for these big particles is probably too small to be detected by this technique.

Magnetic measurements are known to be a more sensitive tool to detect surface effects [20]. The magnetization $M(H)$ of the SSR sample before immersion is linear in field H up to 30 kOe, and the magnetic susceptibility is trivially defined as $\chi = M/H$. The $\chi^{-1}(T)$ curve (not shown here) is similar to the curves that we have already published for this material (see for instance Ref. [7] and references therein), and the Curie–Weiss-law:

$$\chi^{-1}(T) = \frac{C}{T+\theta} \tag{3}$$

is satisfied in the paramagnetic regime, i.e., at temperature greater than the Néel temperature $T_N = 52$ K [34]. For the HTR sample, the magnetization curves are linear in H for $H > 1$ kOe, but at contrast, with the SSR case, they extrapolate to a finite magnetization M_0 in the limit $H \to 0$, as it can be seen in Fig. 13. This feature is characteristics of a residual amount of γ-Fe_2O_3 impurity [6,35]. Although the amount of γ-Fe_2O_3 is very small (less than 0.1% of the product, this extrinsic contribution to the magnetization must be subtracted from the total magnetization to determine the intrinsic magnetic susceptibility that is now defined as $\chi = (M - M_0)/H$. With this definition of χ, Eq. (3) is also satisfied, as it can be seen in Fig. 14. The effective magnetic moment μ_{eff} carried by the iron ions can then be deduced from the Curie constant [20,35]:

$$\mu_{eff} = \left[\frac{3k_B C}{N_A \mu_B^2}\right]^{1/2} = 2.84\, C^{1/2} \tag{4}$$

with N_A the Avogadro number, while C is the Curie constant for one mole of $LiFePO_4$ and μ_B the Bohr magneton. μ_{eff} is in Bohr magneton unit. The result is $\mu_{eff} = 5.38$ and 5.36 for SSR and HTR samples, respectively. The value of μ_{eff} for the samples that do not contain any Li vacancy is in agreement with the theoretical value 4.9 of Fe^{2+} in the high-spin state, but values such as those of SSR and HTR are often met, due a small concentration (lower than 1%) of Li vacancy in the bulk of the $LiFePO_4$ particles [2]. After immersion in water, the magnetic moment of the sinking part increases by 0.04 μ_B in both SSR and HTR samples, to reach $\mu_{eff} = 5.42$ and 5.40, respectively. This value of the magnetic moment is obtained very fast. For technical reasons, the shortest time in which the samples have been investigated is 15 min, where this limit for μ_{eff} was already achieved. The magnetic moment stays as this value even when the samples stay in water for longer times (up to 1 h). This increase of μ_{eff} in the short time limit is the signature of an oxidation of iron from Fe^{2+} to Fe^{3+} at the surface of the samples, the evidence of a delithiation of the surface layer.

To quantify this effect, we first need to model the size distribution of the particles. In absence of aggregation of individual particles, one would have expected a log-normal distribution $f(d)$, i.e., a profile with a single peak in Fig. 2 where the diameters d are reported in abscissa in logarithmic scale. The aggregation, however, leads to the more complex behavior. Instead of being fit by a single Gaussian profile, the distribution is fit as a sum of log-normal

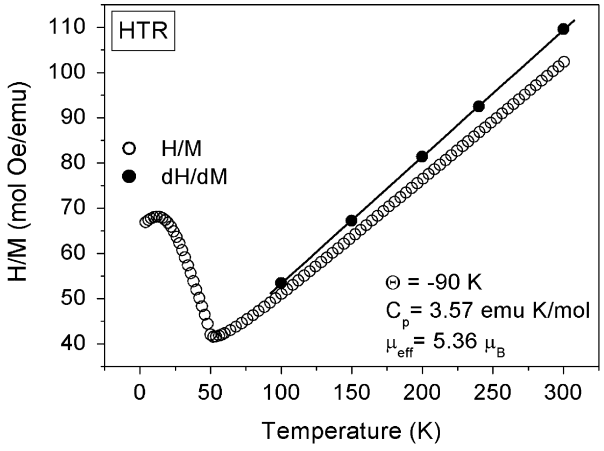

Fig. 14. Inverse of the magnetic susceptibility of the HTR $LiFePO_4$ sample before immersion in water. The open circles are experimental data H/M, with M the magnetization measured in field $H = 30$ kOe. The full circles are the slope dM/dH of the magnetization curves of Fig. 13 in the region $H > 1$ kOe where the variations of M are linear in H.

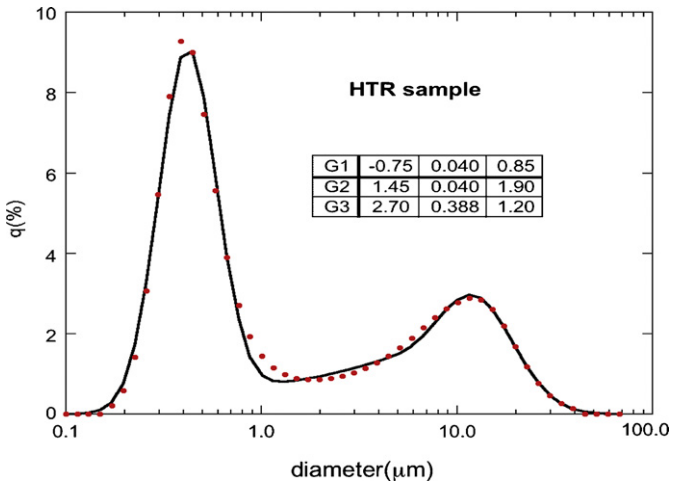

Fig. 15. Fit of the size distribution of the HTR $LiFePO_4$ sample with three Gaussians when ln(d) is chosen as the variable. The parameters: intensity, position, and FWHM for the three Gaussians are also reported.

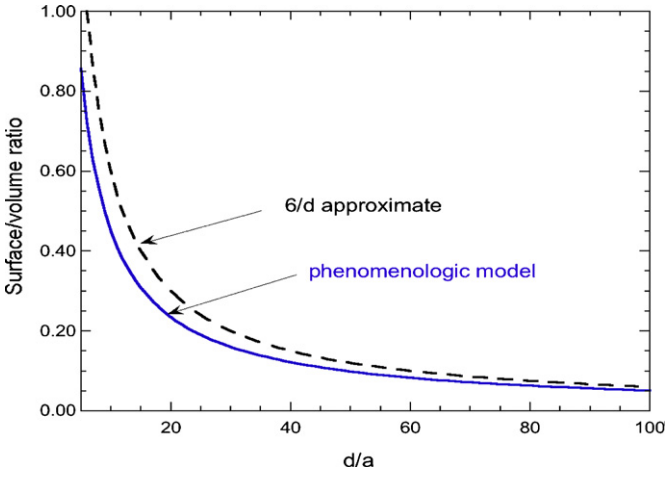

Fig. 16. Surface to volume ratio as a function of the size d of the $LiFePO_4$ particles.

distributions:

$$q(d) = \sum_i f(d; m_i, \sigma_i) = \frac{1}{d}\sum_i G_i[\ln(d)]$$

$$= \sum_i \frac{c_i}{d\sigma_i\sqrt{2\pi}} \exp - \left[\frac{(\ln(d) - m_i)^2}{2\sigma_i^2}\right] \quad (5)$$

We introduced in this equations the distributions G_i that are Gaussian profiles, when ln(d) is chosen as the variable rather than d. The advantage is that the experimental data plotted under the form $dq(d)$ as a function of ln(d) can be fit using the same fitting procedure as the standard one used to fit optical spectra by a set of Gaussian profiles. The result of this fit is illustrated for HTR sample. This sample rather than SSR has been chosen for convenience, since the aggregation is less intricate and three log-normal distributions f (labeled by i) are sufficient to describe the size distribution nicely, as it can be seen in Fig. 15. The parameters of the three Gaussians G_i (i = 1,2,3) are also reported. The intensity (INT) is the pre-factor of the exponential; the position labeled POS in the figure is the parameter m_i, while the last parameter is the full width at half maximum (FWHM), equal to $2\sigma_i[2\ln(2)]^{1/2}$. However, only the first Gaussian G_1 centered at d = 0.39 μm as a physical meaning, the two other Gaussians only mimic the aggregation of the particles. However, SEM experiments show that this aggregation is less important after immersion in water (see Fig. 6), and since the water will presumably be in contact with the particles even in aggregates, by infiltration through the interstitial space, the segregation should not play a significant role in the reaction between particles and water. As a consequence, we mimic the actual size distribution of the particles in contact with water by retaining only the first term (i = 1) in Eq. (5), and renormalize the intensity to keep satisfied the condition:

$$\int f(d)\,\mathrm{d}d = 1 \quad (6)$$

Then, the effective size distribution takes the form:

$$q_e(d) = \frac{1}{d\sigma_1\sqrt{2\pi}} \exp - \left[\frac{(\ln(d) - m_1)^2}{2{\sigma_1}^2}\right] \quad (7)$$

The next step is the determination of the surface/volume ratio $r(d)$ of a particle of diameter d. For this purpose, we follow our previous work [20], according to which we can map this problem to the calculation of $r(d)$ for a particle that crystallizes in the simple cubic lattice with lattice parameter a = 4.17 Å. The result of this calculation is reported in Fig. 16. If d is the effective diameter for an equivalent spherical particle, the s/v ratio is approximated in the large d limit by $\pi d^2/(\pi d^3/6) = 6/d$ (with d measured in a-unit). This law is also shown in Fig. 16 for comparison. The correction for finite size effects is indeed important for nanometer-sized particles, but we are dealing with particles with size large enough so that we found this correction is actually small for the samples investigated here. Then it is straightforward to compute the surface to volume ratio for our sample r_s:

$$r_s = \int \mathrm{d}d\, q_e(d) r(d) \quad (8)$$

The result for HTR sample is

$$r_s = 5 \times 10^{-3} \quad (9)$$

In the following equation x is the fraction of iron ions at the surface that switched from Fe^{2+} to Fe^{3+} states near the interface with water during the immersion process, i.e., switched from magnetic moment 4.90 to 5.40 (in μ_B). For the HTR sample, these iron ions are responsible for the increase of the magnetic moment from 5.36 (before immersion) to 5.40 μ_B (after immersion), which can be written:

$$(5.36)^2 + x[(5.92)^2 - (4.90)^2] = (5.40)^2 \quad (10)$$

Hence x = 0.04 for the HTR sample. Taking Eq. (7) into account, we can then estimate the thickness of the surface layer that has been delithiated:

$$xa/r_s = 3.3\,\mathrm{nm} \quad (11)$$

This is the thickness of the surface layer that we have estimated in our earlier work [20], and also the typical thickness of the disordered surface layer in the TEM images.

The thickness of the layer damaged by the exposition to water, however, is slightly underestimated here, because this calculation deduced from magnetic properties does not take into account the dissolution of Fe and P ions in the water. Analyzing the amount of Fe and P ions reported in Table 1, we find that 1.3% Fe and 3% P (actually PO_4 ions since this unit is very stable) in the SSR sample has been dissolved in the water. This is comparable to the value x = 4% we have found for the fraction of iron ions converted from Fe^{2+} to Fe^{3+} valence states, but still, it is smaller. This result corroborates that the main effect of exposure to H_2O has been the delithiation of the surface layer to form a $FePO_4$ layer that protected the particles against further reaction.

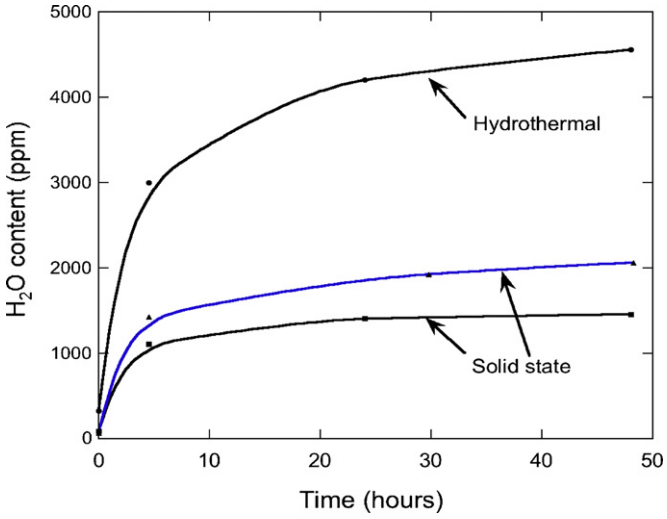

Fig. 17. Moisture content of several C-$LiFePO_4$ samples, expressed in ppm of H_2O with respect to $LiFePO_4$ as a function of time exposure in ambient air at 21 °C (55% relative humidity). The symbols are experimental results. The lines are only guide for the eyes obtained by smooth fit of the data. None of these samples, however, correspond to the HTR and SSR samples investigated in the earlier figures.

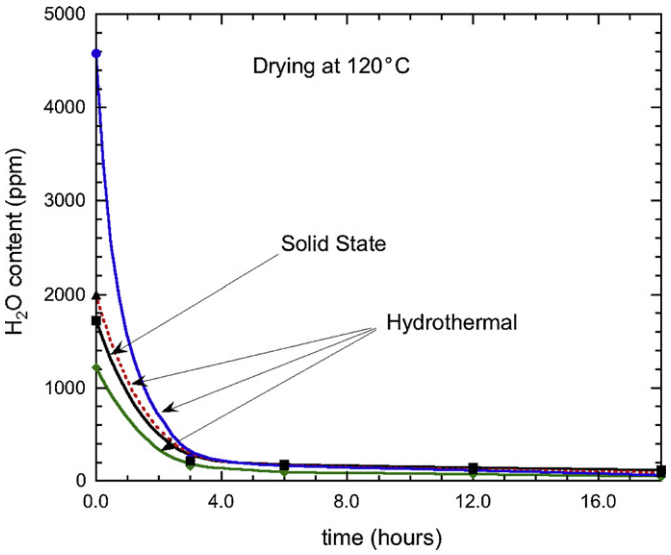

Fig. 18. Moisture content of several C-$LiFePO_4$ samples, expressed in ppm of H_2O with respect to $LiFePO_4$ as a function of time spent in dry atmosphere at 120 °C.

The exposure to water did not generate any remnant magnetization at low temperature. The magnetization of the HTR sample remains the same before and after immersion in water, and that of the SSR sample vanishes before and after immersion. These results mean that immersion in water did not generate Fe_2O_3. Therefore, reactions such as:

$$6LiFePO_4 + 3/4O_2 + 3/2H_2O \rightarrow \mathit{LiFeP_2O_7} + Fe_2O_3 + LiH_2PO_4 + LiOH \quad (12a)$$

$$3LiFePO_4 + 3/4O_2 \rightarrow Li_3Fe_2(PO_4)_3 + 1/2Fe_2O_3 \quad (12b)$$

are ruled out.

3.5. Exposure to air

The evolution of the $LiFePO_4$ surface with time during exposure to H_2O is better investigated in experiments where the material is exposed to ambient air rather than immersion in water. The reason is obviously that the concentration of H_2O that interact with the surface of the particles is much lower in air. In addition, we expect that degradation of the particle surface layer is lower, at least in the timescale of the experiments, because iron ions dissolve in the aqueous solution, but they cannot evaporate. This is another reason why the main effect will be delithiation in the surface layer, as a consequence of the hydrophilic nature of Li. The measurement of the moisture content of the samples exposed to ambient air is an indirect means of investigating this reaction. The results are illustrated in Fig. 17 for several samples. The measurements were performed in a room maintained at 21 °C, in which the relative humidity was 55%. In all cases, quasi-saturation was observed after about 24 h of exposure. However, differences as big as a factor three were observed in the moisture content of samples placed in the same conditions of relative humidity, even for particles prepared by the same process. This observation suggested that the effect of exposure to ambient air also depends on other parameters (homogeneity, porosity, thickness) of the carbon layer that we did not consider in the present work. However, absorption of H_2O is reversible. This is evident in the following experiment. Once the samples are saturated in humid air (left 24 h or more in ambient air), the samples were placed in a dry atmosphere at 120 °C and the moisture content was recorded as a function of time. These results in Fig. 18 show that the samples are dry after 3 h. If the samples are exposed again to ambient air with 55% relative humidity at 21 °C, we recover the results displayed in Fig. 17, and so on. Therefore, the process of absorption/desorption of water is reversible on the scale of few hours. However, the material does not stabilize completely, and exposure of the material to ambient air for a longer timescale of months shows that the reaction with water does not stop, and the electrochemical properties still depend on time, even on the timescale of months.

3.6. Electrochemical measurements

The voltammetry measurements of the SSR and HTR samples (sinking part) after immersion for 1 h in water are reported in Fig. 19. In these measurements, an initial 3.2 V working potential is applied. Then, the voltage was varied at the rate 1.25 mV per minute, as shown in the figure: increase of the voltage up to 4 V, followed by a decrease to 2.2 V, and an increase again up to 3.2 V. Besides the peak associated with Fe^{2+}, the part of the curve obtained by decreasing the voltage shows a secondary peak at 2.63 V that is characteristic of the Fe^{3+} in iron oxide (versus more than 3.5 V in phosphate) [36].

The presence of Fe^{3+} ions in both SSR and HTR samples confirms the delithiation of the surface layer evident in the previous sections. On the other hand, upon increasing the voltage again, this signal disappeared, which shows that the voltammetry curve of the samples before exposure to H_2O was recovered. Therefore, the surface layer was lithiated again during Li insertion, and the effect of immersion in water was reversed. The same holds true for longer immersion times of a few days. In the following experiments, the samples were immersed for 63 h. Then, the samples were dried for 48 h at 85 °C. The electrochemical performance illustrated in Fig. 20 for the HRT sample after drying is the same as that of the sample before immersion, also reported in the figure for comparison. Moreover, it should be noted that the open circuit voltage (OCV) also reported in the figure decreased by 2.3% by immersion in water. Since the OCV is directly related to the state of charge of the battery, it can be viewed as an indirect measurement of the delithiation rate of the battery. Indeed, this result is fully consistent with the 4% delithiation rate deduced from the magnetization

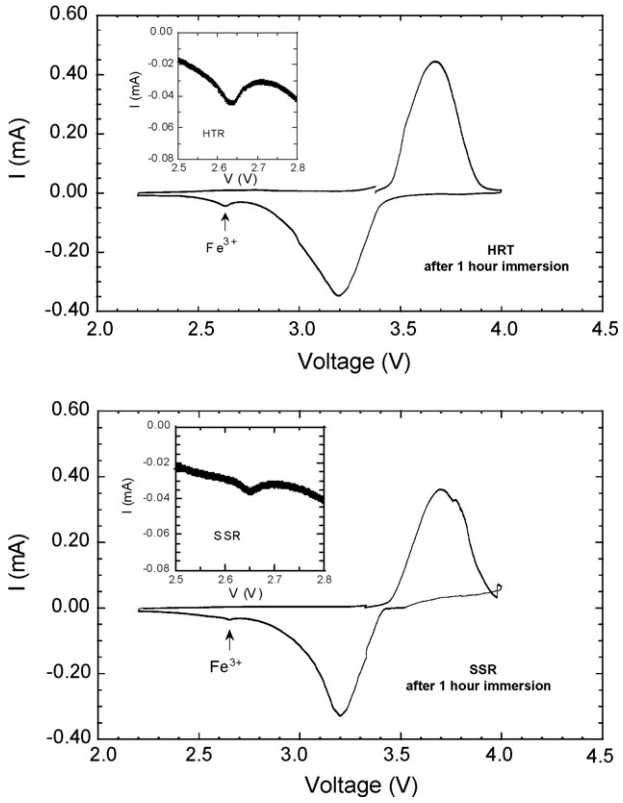

Fig. 19. Voltammetry for the SSR and HTR $LiFePO_4$ samples, after immersion in water during 1 h. The arrows point to the Fe^{3+} peak. The parameters of the measurements are reported in the text.

measurements, and the 1 and 3% loss of Fe and P in the immersion process estimated from the physical and chemical analyses. It thus fully confirms that the delithiation process is located in the surface layer.

The effect of H_2O on the electrochemical properties was also evaluated by exposure of the sample to ambient air. This is illustrated for the HTR sample in Fig. 21 that shows the change of the capacity as a function of time at different temperatures in dry atmosphere and in ambient air (55% relative humidity). The degradation

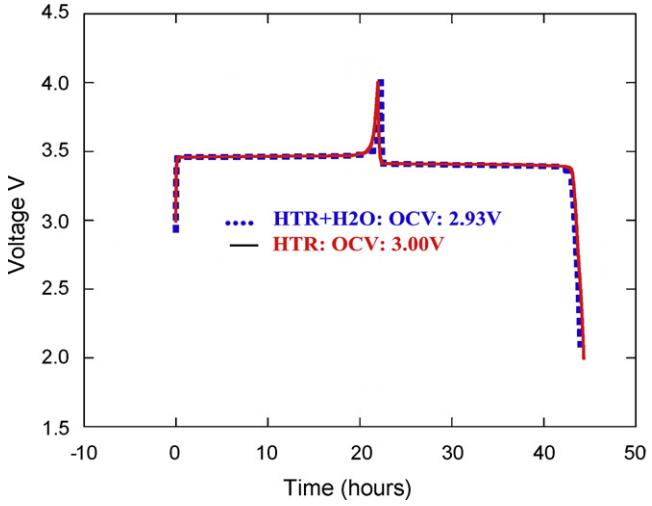

Fig. 20. Electrochemical performance of the C-$LiFePO_4$ (HTR sample)/$LiPF_6$-EC-DEC/Li cells at room temperature. The results are shown before immersion of this sample in water, and after immersion during 63 h, then dried during 48 h at 85 °C.

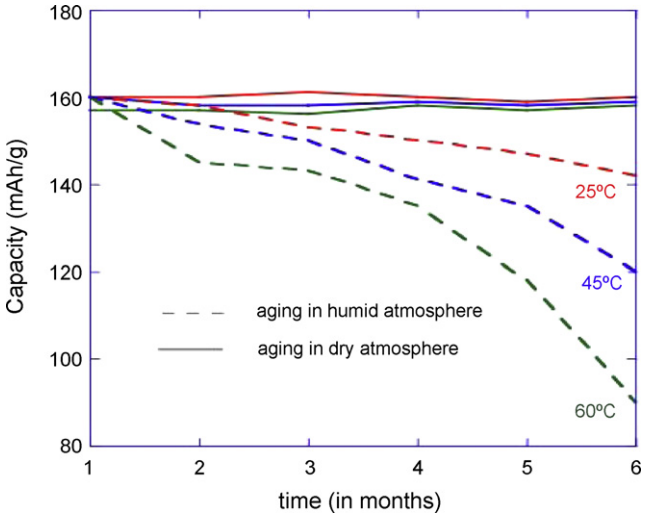

Fig. 21. Capacity of the C-$LiFePO_4$ (HTR sample)/$LiPF_6$-EC-DEC/Li cells as a function of time spent in dry atmosphere and in ambient atmosphere (55% relative humidity), at three different temperatures. The temperatures at which the full curves (in dry atmosphere) have been obtained (in color in the web version) can be distinguished by the fact that they do not overlap, and the property that the lower the temperature, the higher the capacity is.

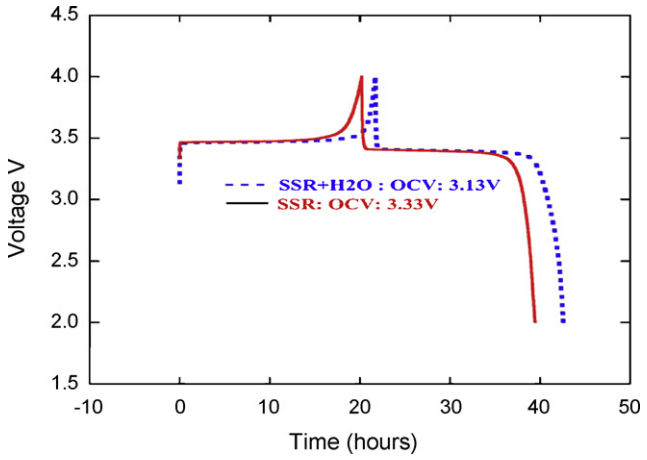

Fig. 22. Electrochemical performance of the C-$LiFePO_4$ (SSR sample)/$LiPF_6$-EC-DEC/Li cells at room temperature. The results are shown for a cell prepared with the sample before immersion in the water for reference, and with the sample after immersion in water for 63 h and dried during 48 h at 85 °C, but then stored in ambient air for 6 months, at contrast with the case reported in Fig. 20.

rate increases with temperature and becomes dramatic at the scale of 6 months. This degradation is evident by the experiments displayed in Fig. 20 for samples with the same treatment as before (immersion for 63 h, followed by drying at 85 °C for 48 h), but then left for 6 months in the laboratory. The result is illustrated for the SSR sample in Fig. 22. The material was aged for 6 months, resulting in an important loss in capacity and OCV voltage. As far as the lithiation process cures the degradation in a first charge/discharge cycle, as it is the case for exposure to H_2O during few days, the inconvenience is minor, but on the long time scale of 6 months, our results show that the material must be stored under dry conditions to protect it against moisture.

4. Concluding remarks

The effect of water on the stability of carbon-coated $LiFePO_4$, prepared by solid-state reaction (SSR), and hydrothermal (HTR)

synthesis, was investigated by a variety of experimental techniques such as XRD, TEM, SEM, FTIR, particle size analysis and magnetic measurements. The samples were contacted with liquid water or humidity in ambient air. Cyclic voltammetry was used to characterize the electrochemical properties of carbon-coated $LiFePO_4$ in 1 M $LiPF_6$ in ethylene carbonate (EC) + diethylene carbonate (DEC).

A major finding of this study is that the carbon coating does not protect $LiFePO_4$ when exposed to H_2O. In the extreme case where the $LiFePO_4$ particles, which are obtained by SSR and HTR processes, are immersed in water, part of the carbon detaches from the particles and floats to the surface. The effectiveness of the carbon coating to protect $LiFePO_4$ particles against moisture is better tested by the milder exposure of the particles to humid ambient air. On average, the carbon-coated $LiFePO_4$ from solid-state reaction synthesis produces a carbon coat that is more protective than that from the hydrothermal process.

The reaction of $LiFePO_4$ with H_2O is limited to the surface layer when the time scale of exposure to water is short (days in case the material is immersed in water, months in the case of exposure to the moisture of ambient atmosphere). On this time scale, the main effect is delithiation resulting from the strong reaction of Li with H_2O, however, lithium is lithiated in the first discharge of the $LiFePO_4$ electrode. However, the reaction of $LiFePO_4$ and H_2O appears to be more complex than simply a delithiation process, since the immersion in water results in the dissolution of iron and phosphate compounds in the aqueous solution. After long-term exposure, this reaction definitely alters $LiFePO_4$ and its electrochemical performance, even when it is only exposed to the relative humidity of ambient air instead of being immersed in water.

Similar effects of water and air exposure were observed with other cathodes for rechargeable lithium batteries, but not on the lithiated phosphates. The interaction of unlithiathed phosphates with water has been investigated in many works in different contexts, but the comparison with the present case is mixed because the reaction of our product with water is clearly due to the presence of Lithium ($FePO_4$ das not react). Among Lithium compounds, the exposure to moisture of $LiNi_{1-x-y}Co_xMn_yO_2$, an active material known for this ability to reach capacities larger than 2400 mAh g^{-1} with a 4.2-V cut-off, was investigated. For $1-x-y>0.8$, the rapid reaction of this product with air results in the formation of Li_2CO_3 and LiOH on the surface [37–39]. The formation of LiOH was observed on the surface of $LiNiO_2$ as well [40]. In the present work, the presence of LiOH on the $LiFePO_4$ surface exposed to air and/or immersed in water is clearly evident. In the case of $LiNiO_2$, the formation of LiOH was attributed to the reaction:

$$LiNiO_2 + yH_2O \rightarrow Li_{1-y}NiO_{2-y/2} + yLiOH \quad (13)$$

which involves the evolution of oxygen. With $LiFePO_4$, the evolution of oxygen is precluded because of the strong covalent bending in the phosphate PO_4^{3-} unit. The formation of LiOH then presents a more general trend of Li-intercalation compounds that does not necessarily require the migration of oxygen ions [40]. The surface reaction mechanism of $LiNiO_2$:

$$2Li^+ + CO_3{}^{2-}/2OH^- \rightarrow Li_2CO_3/2LiOH \quad (14)$$

was attributed to the presence of NiO impurity, indicating this reaction is specific to this Ni-compound [41].

Zuhang et al. reported the presence of Li_2CO_3 on the surface of $LiNi_{0.8}Co_{0.15}Al_{0.005}O_2$ powder exposed to air [39], and long-term exposure produced a dense Li_2CO_3 coating approximately a few nm thick, which severely reduces the capacity in an irreversible manner [39]. However, physical and chemical analysis of the surface of $LiFePO_4$ in the present work was focused on samples that were exposed to moisture for rather short times where the electrochemical properties remain reversible. Similar analyses are being considered with $LiFePO_4$ cathodes that are exposed for a long time (i.e., few months) to assess if the irreversible loss of capacity has the same origin as in $LiNi_{0.8}Co_{0.15}Al_{0.005}O_2$. That is, a Li_2CO_3 coating of $LiFePO_4$, or a different coating more specific to the phosphate compound, such as a Li_3PO_4 coating, for instances.

The hygroscopic character of $LiFePO_4$ can be compared with that of $LiNi_{0.83}Co_{0.15}Al_{0.005}O_2$ [42]. When $LiNi_{0.83}Co_{0.15}Al_{0.005}O_2$ is exposed to air with relative humidity 50% for 48 h, the moisture content was 1270 ppm. When this air-exposed material was heat-treated at 700 °C for 2 h, the moisture content in the powder decreased to 250 ppm, but increased to 2576 ppm after exposure to air again. This moisture content is in between the value we found for $LiFePO_4$ prepared by hydrothermal and solid-state reactions (see Fig. 15). For comparison, the moisture content measured for $LiCoO_2$ is in the range 100–300 ppm [42]. Therefore, $LiFePO_4$ must be protected against humidity when stored for a few months.

After this work, we recommend the storage of $LiFePO_4$ in a glove box for university and academic research, and in a dry room at less than 5% RH. We also recommend drying the electrode in vacuum at 120 °C for industrial use.

Acknowledgement

The authors like to acknowledge R. Veillette and Dr. P. Hovington from IREQ for the SEM and TEM pictures.

References

[1] A.K. Padhi, K.S. Nanjundaswamy, J.B. Goodenough, J. Electrochem. Soc. 144 (1997) 1188.
[2] K. Zaghib, A. Mauger, J. Goodenough, F. Gendron, C. Julien, Chem. Mater. 19 (2007) 3740.
[3] N. Ravet, Y. Chouinard, J.F. Magnan, S. Besner, M. Gauthier, M. Armand, J. Power Sources 97–98 (2001) 503.
[4] N. Ravet, S. Besner, M. Simoneau, A. Vallée, M. Armand, J.F. Magnan, US Patent 6,962,666 and 6,855,273 (1999).
[5] M. Armand, M. Gauthier, J.-F. Magnan, N. Ravet, World Patent WO 02/27823 A1 (2002).
[6] A. Ait-Salah, A. Mauger, C.M. Julien, F. Gendron, Mater. Sci. Eng. B 129 (2006) 232.
[7] C.M. Julien, A. Mauger, A. Ait-Salah, M. Massot, F. Gendron, K. Zaghib, Ionics 13 (2007) 395.
[8] N. Ravet, C. Michot, G. Nuspl, G. Liang, M. Gauthier, Proceedings of the 210th ECS Meeting, Cancun, Mexico, 2006.
[9] A. Mauger, A. Ait-Salah, M. Massot, F. Gendron, K. Zaghib, C.M. Julien, ECS Trans. 3-36 (2007) 57.
[10] K. Zaghib, N. Ravet, A. Mauger, M. Gauthier, J.B. Goodenough, C.M. Julien, ECS Trans. 3-27 (2007) 119.
[11] J.F. Martin, A. Yamada, G. Kobayashi, S.-I. Nishimura, R. Kanno, D. Guyomard, N. Dupre, Electrochem. Solid State Lett. 11 (2008) A12.
[12] See, for instance, the report on chemical properties, health and environmental effects of lithium: http://www.lenntech.com/Periodic-chart-elements/li-en.htm.
[13] D.Y.W. Yu, K. Donoue, T. Kadohata, T. Maruta, S. Matsuta, S. Fujitani, J. Electrochem. Soc. 155 (2008) A526.
[14] M. Manickam, P. Singh, S. Thurgate, K. Prince, J. Power Sources 158 (2006) 646.
[15] K. Zaghib, Proceedings of the BATT Review Meeting, Berkeley, 2003.
[16] W. Porcher, P. Moreau, B. Lestriez, S. Jouanneau, D. Guyomard, Electrochem. Solid-State Lett. 11 (2008) A4.
[17] J. Cournot, J. Bary, C. R. Acad. Sci. (Paris) 190 (1930) 1426.
[18] G. Chen, X. Song, T.J. Richardson, J. Electrochem. Soc. 154 (2007) A627.
[19] T.J. Richardson, Proceedings of the 3rd Annual Conference on Lithium Mobile Power Advances in Lithium Battery Technologies for Mobile Applications, San Diego, USA, 2007.
[20] K. Zaghib, A. Mauger, F. Gendron, C.M. Julien, Chem. Mater. 20 (2008) 462.
[21] A. Ait-Salah, A. Mauger, K. Zaghib, J.B. Goodenough, N. Ravet, M. Gauthier, F. Gendron, C.M. Julien, J. Electrochem. Soc. 153 (2006) 1692.
[22] K. Zaghib, M. Armand, HQ Internal Report (1997) and 1st PBFC, Jeju, Korea (2003).
[23] S. Yang, P.Y. Zavalij, M.S. Whittingham, Electrochem. Commun. 3 (2001) 505.

[24] See, for instance: http://www.lasurface.com/database/elementxps.php (in French).
[25] J.-F. Berret, O. Sandre, A. Mauger, Langmuir 23 (2007) 2993.
[26] Intermediate steps in the phosphatation of iron can be found for instance on the web site http://www.france-traitement.com/fr/phosphatation_fer.html (in French).
[27] S. Okazaki, N. Ohtori, I. Okada, J. Chem. Phys. 91 (1989) 5587.
[28] P. Jozwiak, J. Garbarczyk, A. Mauger, F. Gendron, C. Julien, J. Non-Cryst. Solids 354 (2008) 1915.
[29] N. Ravet, M. Gauthier, K. Zaghib, A. Mauger, J.B. Goodenough, F. Gendron, C. Julien, Chem. Mater. 19 (2007) 2595.
[30] M.T. Paques-Ledent, P. Tarte, Spectrochim. Acta A30 (1974) 673.
[31] C.M. Burma, R. Frech, J. Electrochem. Soc. 151 (2004) 1032.
[32] See, for instance, G. Nagalakshmi, J. Pharm. Sci. 6 (2007) 69.
[33] A. Zaban, D. Aurbach, J. Power Sources 54 (1995) 289.
[34] R.P. Santoro, R.E. Newnham, Acta Crystallogr. 22 (1967) 344.
[35] A. Guerfi, M. Kaneko, M. Petitclerc, M. Mori, A. Zaghib, J. Power Sources 163 (2007) 1047.
[36] H. Sakaeke, S. Higuchi, K. Kanamura, H. Fujimoto, Z. Takehara, J. Electrochem. Soc. 142 (1995) 360.
[37] S.W. Song, G.V. Zhuang, P.N. Ross Jr., J. Electrochem. Soc. 151 (2004) A1162.
[38] K. Matsumoto, R. Kuzuo, K. Takeya, A. Yamanaka, J. Power Sources 81–82 (1999) 558.
[39] G.V. Zhuang, G. Chen, J. Shim, X. Song, P.N. Ross Jr., T.J. Richardson, J. Power Sources 134 (2004) 293.
[40] R. Moshtev, P. Zlatilova, S. Vasilev, I. Bakalova, A. Kozawa, J. Power Sources 21 (1999) 434.
[41] H.S. Liu, Z.R. Zhang, Z.L. Gong, Y. Yang, Electrochem. Solid State Lett. 7 (2004) A190.
[42] J. Cho, Y. Kim, in: S.S. Zhang (Ed.), Advanced Materials and Methods for Lithium-Ion Batteries, Transworld Research Network Publ, 2007, p. 49.